AIChE WILEY InterScience DISCOVER SOMETHING GREAT

Effect of Vibration on Flow Properties of Fine Glass Beads

C. Soria-Hoyo, J. M. Valverde, and A. Castellanos
Faculty of Physics, University of Seville, Avenida Reina Mercedes s/n, 41012 Seville, Spain

DOI 10.1002/aic.11423
Published online February 28, 2008 in Wiley InterScience (www.interscience.wiley.com).

An estimation of cohesion C and angle of internal friction φ of fine glass beads, which have been previously subjected to small intensity vertical vibrations of controlled frequency and amplitude for a fixed period of time, is presented. In the range of vibration intensities tested previbration causes powder compaction. Experimental measurements to obtain C and φ have been performed by means of a centrifuge powder tester in which the previbrated powder bed is rotated around its vertical axis. At a critical rotation velocity the shear stress induced by rotation is large enough to drive material avalanches. From a theoretical analysis of these avalanches, based on the Coulomb's method of wedges, C and φ are derived. We have found a significant increase of cohesion, and a slight decrease of the angle of internal friction as the effective consolidation stress due to previbration is increased. The estimated interparticle cohesion force f_t from the experimental measurements, and using a Rumpf's averaging equation, is in agreement with the calculated interparticle attractive force due to van der Waals and capillary interaction for the unconsolidated beds. Moreover f_t increases as the effective consolidation stress is increased in agreement with estimations from theoretical models based on contact plasticity. This result suggests that, at the microscopic level of asperities, compaction due to previbration is able to induce plastic deformation of the contacts. *AIChE J,* 54: 886–896, 2008
Keywords: particle technology, particulate flows, rheology

Introduction

Vibration is commonly present in industry in the handling and transporting powders. Thus, the understanding of how the powder behavior is affected when subjected to vibrations would provide valuable design information. The standard vibration experiment consists of a powder in a container mounted on a rigid base, which is subjected to mechanical vibrations. For deep beds this simple experiment exhibits a rich phenomenology depending on the intensity and direction of vibration, from compaction[1] at small vertical vibration intensities, to fluidization at high-vibration intensities,[2] passing through convective instability as first discovered by Faraday.[3]

Correspondence concerning this article should be addressed to J. M. Valverde at jmillan@us.es.

Small intensity vertical vibration of a loosely packed bed induces compaction by helping grains to overcome arches and other barriers.[1] The compaction induced by vibrations is extremely difficult to understand from pure theoretical grounds since extrapolating macroscopic properties from the underlying microscopic behavior is fairly more difficult with powders than with liquids and gases. Researchers have mostly focused on the time dependence of the compaction process, and also on how much settling occurs as a function of the initial state and vibration intensity.[1,4] Since what happens is so diverse, the common strategy has been to study the behavior of ideal beds of noncohesive coarse grains. Usually, the vibration intensity has been parameterized by Γ, the ratio of the peak acceleration to the gravitational acceleration. Nowak et al.[1] observed that a vibrated bed of millimeter-sized glass beads evolves from an initial, loose configuration (particle volume fraction $\phi \simeq 0.59$) to a close packed configuration ($\phi \simeq 0.63$) when the vibration intensity

was ramped up from zero to $\Gamma \simeq 4$. Ramping the vibration intensity repeatedly up and back down again revealed that the compaction process induced by vibration was irreversible.[1] On the other hand, in the branch of high-vibration intensities ($\Gamma \gtrsim 4$), the increase of the vibration intensity caused a monotonic and reversible decrease of ϕ.

Industry concerns are mainly focused on fine cohesive powders. Most of the processing plants dealing with fine powders experiment handling problems because of the lack of material flow predictability.[5] While the large ratio of surface area to volume of fine powders provides high-fluid-solid contact and reaction efficiencies, the relative strength of interparticle attractive forces is also increased, giving rise to poor flowability[6] that is unpredictably affected by vibrations during powder transportation or storage when used is resumed. The Jenike shear cell[7] has been widely used to measure the angle of internal friction and cohesion of cohesive powders. Essentially the method consists of compacting a sample with a known external load into a cylindrical cell composed of two metal rings one upon the other. With the compaction load still applied the minimum steady-state shear stress necessary to displace the upper ring horizontally with respect to the lower one is measured. According to the Mohr-Coulomb criterion, the angle of internal friction φ, and the cohesion C of the powder are a measure of its capability to sustain shear stresses, and, therefore, to flow.[8] Consider an arbitrary plane through the sample and a shear stress τ acting on that plane; there will be a critical value of the shear stress that will cause the material to shear off in that plane. This yield stress depend on the normal stress σ acting perpendicular to the plane. In his pioneer work, Coulomb approximated the relationship between τ and σ by a linear function[8,9]

$$\tau = \sigma \tan \varphi + C \tag{1}$$

Equation 1 defines the Mohr-Coulomb yield locus of the granular material. Applications to avalanche data have demonstrated that the Coulomb model successfully captures the relevant features of avalanche motion of cohesive powders.[10,11]

The effect of vibration on the yield loci of cohesive powders was investigated recently by Kollmann and Tomas[12] using limestone and titania powder, and, previously, by Roberts and Scott[13] using pyrophyllite and iron ore, and Arnold[14] using iron ore fines. In refs. 12 and 13 the setup consisted of a modified Jenike shear cell fitted with a vibration exciter, which was designed to permit the shear strength to be measured during the application of horizontal vibrations (parallel to the plane of shear). Kollmann and Tomas[12] distinguished between vibrations applied only during shear (method A), and vibrations applied during preshear (method B). A main result from these works was that the horizontal vibrations leaded to a significant reduction of the cohesion, whereas the angle of internal friction did not experience a significant variation. These studies were focused on situations in which horizontal vibrations do not induce powder compaction, but instead are used to promote and control gravity flow. The study of the effect of these types of vibrational excitations is indeed relevant for applications, such as pulsed vibration, as used for bridge breaking and discharging (method A), and continuous vibration during discharge, as used in vibrated hoppers (method B). Another method of excitation, consisting of vibration during preconsolidation (method C) was not addressed, although the authors recognized that this study has a great potential interest for applications, such as undesirable vibration during silo filling and storage. Arnold[14] measured the yield loci of iron ore fines using the normal Jenike procedure, and looked at the effect of a vertical vibration of the top ring of the cell. It was observed that vibrations, applied perpendicular to the plane of shear, not only caused appreciable consolidation of the powder, but also a significant increase in its cohesion.

A problem of using the modified Jenike cell to investigate the flow properties of powders is that, in applications involving powder flow, the sample is usually in a state of small consolidation (typically in a range from a few Pa to a few hundred Pa), while in the Jenike shear cell the sample is initialized in a state of consolidations typically larger than 1 kPa. The Schulze ring shear tester[15] is a technical improve on the Jenike tester. This method is able to measure the yield locus at small consolidations, and has been recognized as a standard technique for powder flow diagnosis.[16] A general problem that besets shear testers is that, in order to relate the stresses to the real stresses inside the material, it must be assumed that the shear process takes place uniformly throughout the sample,[17] which is known to be false for overconsolidated materials.[17] In the case of highly cohesive powders, the shear occurs through fracture surfaces of uncertain location that are difficult to be erased by the initialization procedure used in the shear testers. The interested reader may see ref. 18 for an extensive review on measuring techniques and instruments, including shear testers and also split cell testers designed to measure just cohesion.

In our experimental work we have estimated experimentally the angle of internal friction and cohesion of powder samples compacted by previous vertical vibration. Measurements have been carried out by means of a centrifuge powder tester (CPT).[19] This device has been described in detail in ref. 20, in which results from measurements on diverse powders were also shown to illustrate its functioning. For the reader's convenience we give also in this article a summary of the setup and procedure.

Experimental Setup

In the experimental setup the sample of granular material partially fills a rectangularly shaped container of internal length $2R = 8$ cm and 0.6 cm depth. The material is initialized by gently shaking the container horizontally to smooth the sample free surface and make it horizontal. After initialization, the container is mounted on an electromagnetic vibration exciter driven by a signal generator, which provides sinusoidal, vertical vibrations of controlled frequency ν and amplitude A. The vibrator (model Tira vib TV52120) is powered by a power amplifier (model Tira BAA500), with a maximum output of 6 A. The acceleration amplitude of the container is monitored using a piezoelectric accelerometer (Bruel and Kjaer model 4500A) attached to its base. The current output of the accelerometer is read using a lock-in amplifier (Stanford Research Instruments model SR530) tuned to the frequency of the vibrations. Thus, open loop control was used to set the amplitude of the vibration. During the

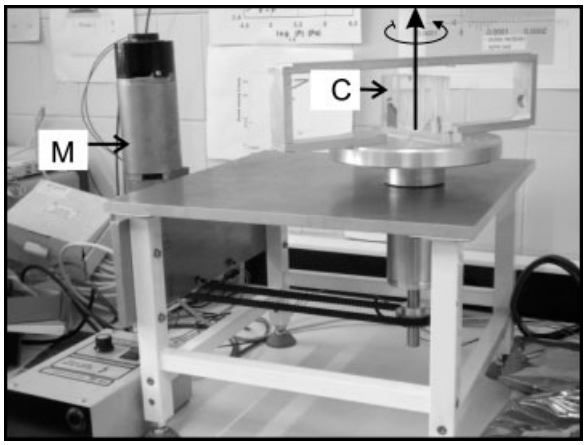

Figure 1. Device built at the University of Seville to measure the angle of internal friction and cohesion of granular materials.

The granular material rests on a rectangular cell (C) which is fixed to a rotatory plate. The motion is driven by a motor (M), which is controlled by a computer. A wireless camera (not shown) fixed to the rotatory structure records the evolution of the material as the cell is rotated.

previbration procedure the sample is subjected to vertical oscillations at fixed amplitude and frequency for a time period of two minutes. Experiments have been performed at two selected frequencies (200Hz and 1kHz), which are controlled to within ± 0.1 Hz.

We have tested soda-lime glass beads of dia. $d_p \simeq 40 \pm 10$ μm, and particle density $\rho_p \simeq 2{,}500$ kg/m^3. The sample masses used to run the experiment are between 2 and 4 grams, corresponding to typical volumes between 1.5 cm^3 and 3 cm^3. The height H of the material layer in the container is between 3 and 5 mm, that is the powder layer can be classified as a deep bed ($H/d_p \gtrsim 100$). The dimensionless peak acceleration amplitude $\Gamma = A(2\pi\nu)^2/g_0$, where $g_0 = 9.81$ m/s^2 is the acceleration due gravity, is in a range that extends up to $\Gamma \simeq 5$, and can be controlled to within $\pm 0.1 g_0$. Although the time average of the instantaneous vibrational acceleration is zero, when ramping up the vibration intensity we observe irreversible compaction of the powder layer that remains all the time attached to the base of the container. Thus, it can be said that the net effect of vibration within the applied range of intensities is to increase the effective acceleration on the sample by a factor $(1 + \Gamma)$. The consolidation stress σ_{c0} of the nonvibrated sample, which is only due to its own weight, is small (typically $\sigma_{c0} \simeq \rho_p \phi g_0 H \simeq 40$ Pa). By means of previbration, the effective consolidation stress $\sigma_c \simeq \sigma_{c0}(1 + \Gamma)$, is, thus, increased in a range extending up to $\sigma_c \simeq 400$ Pa.

Once the powder is compacted by vibrations it is carefully taken to the centrifuge powder tester (CPT). In Figure 1 we show a photograph of the CPT built at the University of Seville. The container is placed on a rotatory table, and it is rotated around its vertical axis. The rotation velocity is driven by a D.C. permanent magnet motor controlled by a computer. In the experiments reported in this article the rotation velocity was steadily increased at a rate of 1 rpm/s up to a maximum value of 600 rpm. At a critical point the shear stress caused by the action of the centrifugal force is large enough to drive material avalanches. The succession of avalanches are recorded by a wireless TV cam solidary to the container and later analyzed with the help of an image software to obtain the mechanical properties of the material as a function of previbration intensity.

In order to compare our results with results from independent experiments we have tested the powder by using the Schulze ring shear tester (model RST-01.pc computer-controlled), which is recognized as a standard shear test method for bulk solids.[16] The detailed principle of the ring shear tester can be seen in ref. 15. Figure 2 shows the yield loci measured for different values of the maximum normal stress $\sigma_{\max}$ initially applied by the lid on the powder. From this figure it can be concluded that the behavior of the powder can be well described by the Coulomb yield condition (Eq. 1), with an angle of internal friction φ around 25^0 that decreases slightly as $\sigma_{\max}$ is decreased (see Figure 2b). In Figure 2b we have plotted also the cohesion calculated from the yield loci as a function of $\sigma_{\max}$. It is seen that the cohesion increases as the maximum normal stress is increased. Mea-

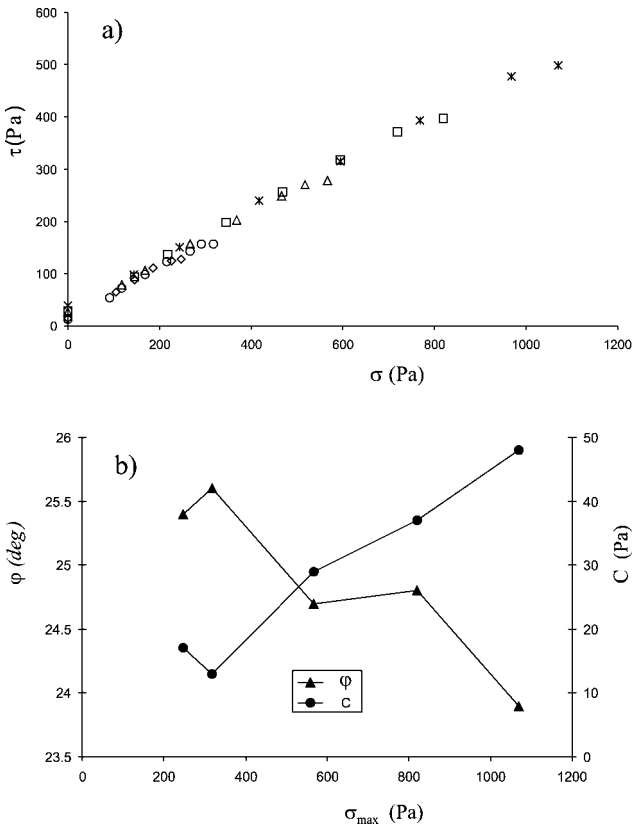

Figure 2. (a) Yield loci measured for the fine glass beads and for different values of the maximum normal stress applied by a lid using the standard Schulze ring shear tester; (b) angle of internal friction (left axis) and cohesion (right axis) derived as a function of the maximum normal stress.

The typical indeterminacy in the measurement of φ is around 1^0, and it is around 10 Pa in the measurement of C.

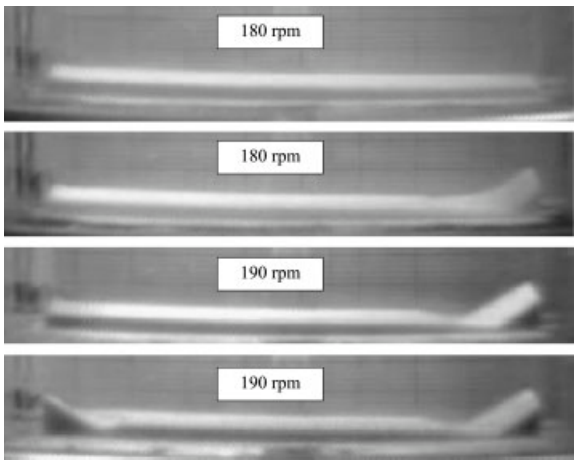

Figure 3. Sequence of photograms illustrating the occurrence of the first avalanche in the centrifuge powder tester at a rotation velocity ω = 180 rpm in the right side, and at ω = 190 rpm in the left side.

surements for σ_{max} below 200 Pa were not possible with sufficient accuracy.

Centrifuge Powder Tester

The CPT is based on the analysis of the critical state of stresses leading to avalanches in a rotating layer of powder. Figure 3 shows a sequence of photograms that illustrate the occurrence of the first avalanche. In our analysis the rotation velocity $\omega = \omega_c$ at which this first avalanche occurs will serve us to derive the cohesion of the granular material. In practice, the initial surface of the material is not perfectly horizontal if the initial state is not perfectly homogeneous. Thus, the first avalanche happens at smaller (larger) values of ω_c if the slope at the side of the cell is slightly inclined downward (upward). This problem is aggravated if the surface heaping phenomenon, which is usual at low-vibration frequencies,[21] appears caused by previous vibration. In Figure 4 we show a single peak occurring to one side of the container as a consequence of vibration induced heaping. When the occurrence of this phenomenon was observed, the experimental data on ω_c were just discarded.

After the first avalanche has taken place, and in the range of high-rotation velocities ($\omega \gtrsim 300$ rpm for the glass beads tested in this work), the free surface of the material slopes against the lateral wall. As ω is further increased the slope becomes unstable and thin avalanches take place that progressively increase the stable angle of the slope (see Figure 5). In our analysis, the first step will be to measure the angle of the slope at high-rotation velocities in order to derive the angle of internal friction of the granular material.

Theoretical analysis

We now turn to summarize the theoretical analysis of the experimental observations in order to develop a methodology for obtaining the experimental values of the cohesion and angle of internal friction. Our analysis is based on the Coulomb method of wedges.[22] The underlying assumptions in the method of wedges are (1) that failure occurs along a slip

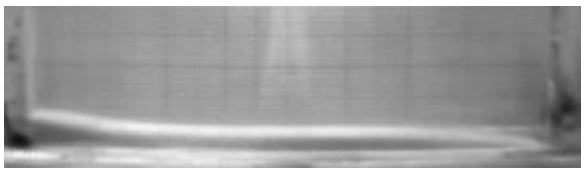

Figure 4. Photograph taken just after vibration of the bed illustrating the occurrence, in this particular case, of surface heaping during the previous vibration process (Γ = 4.4, ν = 200 Hz).

When surface heaping during previbration occurred the sample was discarded.

surface which is composed of planar surfaces, (2) that the stresses at the slip surface reach the critical yield condition specified by the Coulomb's yield locus (Eq. 1), and (3) that the condition of critical equilibrium holds i.e., just before the avalanche, we assume a balance of forces acting on the sliding wedge. The method is commonly applicable to two-dimensional (2-D) situations. In our experiment, since the depth of the cell is small as compared to its length, the stress state of the sample can be approximately considered as 2-D. We also neglect the interaction between the material and the wall, as long as the area of the slip surface is large as compared to the area of contact between the sliding wedge and the wall.

First Avalanche. Let us first use the method of wedges to analyze the first avalanche in the rotating cell. Figure 3 shows the post-avalanche profile that indicates that the sliding wedge involves a portion of material of a certain depth located at the outer region. As a first approximation we consider a simple triangular wedge model composed of two smaller subwedges as shown in Figure 6. In this case the slip surface is approximated just by two intersecting slip planes. The geometry of the wedge is determined by two parameters,

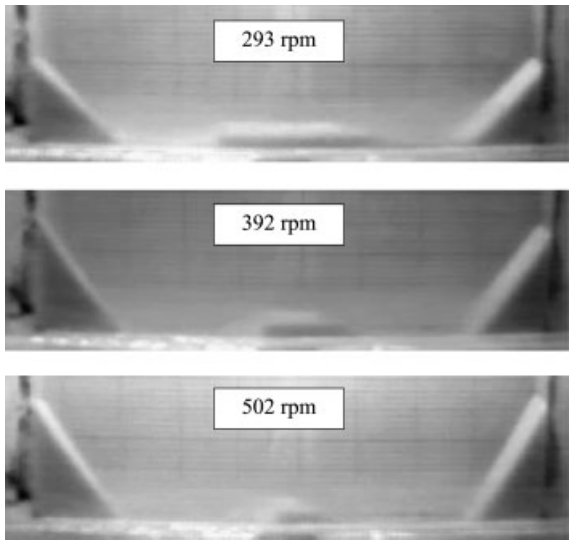

Figure 5. Photograms illustrating the increase of the angle of stability of the slope against the side walls of the container as the rotation velocity in the centrifuge powder tester is increased (Γ = 1.2, ν = 200 Hz).

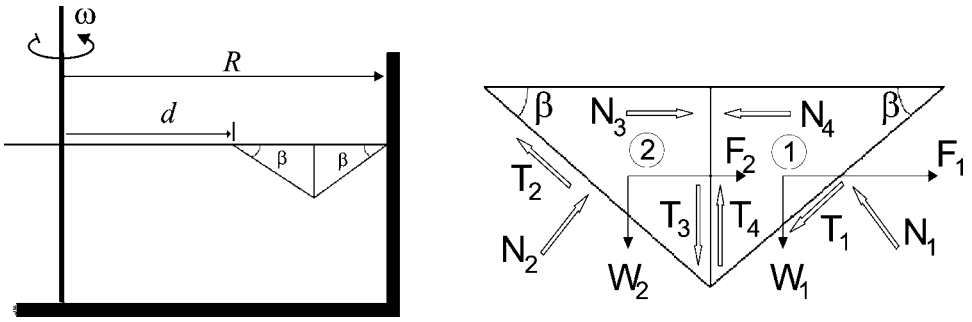

Figure 6. Theoretical composite wedge.

The fracture surface is assumed to be composed of two planes, inclined at an angle β. Normal (N_i), and tangential (T_i) forces per unit depth acting on the planar slip surfaces, as well as weight (W_i), and centrifugal (F_i) forces per unit depth on the sliding wedge are represented in the magnification shown in the right side.

the angle β, and the distance to the axis of rotation d. On each subwedge the condition of static equilibrium must apply (i.e., the sum of forces must equal zero). Also, along each slip surface the Coulomb yield condition must be satisfied. In summary, we have a total of nine equations that must be satisfied with eight unknowns, which correspond to tangential and normal forces on the slip planes. The compatibility condition of this system yields a functional relation $\omega = \omega(\beta,d)$ between the rotation velocity ω, and the wedge parameters β and d (see Appendix). The function $\omega(\beta,d)$ presents a minimum at given values of β_0 and d_0. Once the minimum rotation velocity, making possible the critical equilibrium, is reached, the material avalanches according to the theory. Then we must find the minimum value of ω, which is the solution of critical equilibrium equations.

The results of the Coulomb method of wedges are only approximate since the actual slip surface will be generally curved. By increasing the number of planar slip surfaces the accuracy of the method can be improved.[22] Thus, a model of three slip planar surfaces will allow us to improve the accuracy of the method. Figure 7 shows a more realistic composite wedge. We have now a total of three subwedges composing the theoretical wedge, which is determined by three independent parameters (β, d and l). Proceeding in a similar way to the previous calculation we arrive at a compatibility condition for critical equilibrium $\omega = \omega(\beta,d,l)$. The smallest value of ω at which this condition is fulfilled is the rotation velocity at which the model predicts the first avalanche.

We have checked that the difference between results of the two former models is, at most, of the order of 5%, which is in general smaller than the experimental scatter. Thus, the three-slip-plane model is accurate enough, and it is not practical to seek for further mathematical complication. Note, however, that just equating the experimental rotation velocity for the first avalanche to the theoretically predicted one allows us to determine only one material property, either the angle of internal friction φ, or the cohesion C. Thus, we need to know before hand one of them from an independent measurement. In the next section we describe how φ can be derived from the stable angle of the slope measured at high rotation velocities (Figure 5).

Angle of the Slope at High-Rotation Velocities. Figure 8 shows the simple wedge model proposed for predicting the angle of stability of the slope of material deposited against the lateral wall at high rotation velocities. Note that this wedge model must differ from the wedge model used for the first avalanche, since in the latter case the surface of the free surface was horizontal, while in the former the free surface is already inclined before avalanching. The angle θ is the angle of the slope before the avalanche takes place. The slip surface is inclined at an angle α that will be the stable angle of the slope after the material has avalanched. F is the centrifugal force per unit depth acting on the wedge, and W is its weight per unit depth. T and N represent the tangential

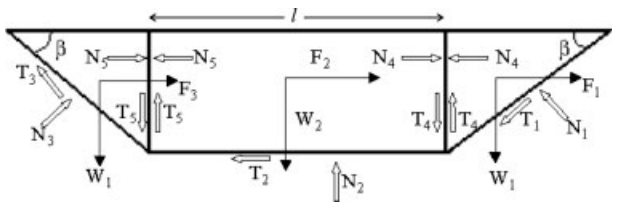

Figure 7. Magnified theoretical composite wedge.

The fracture surface is assumed to be composed of three planar surfaces. Normal (N_i), and tangential (T_i) forces per unit depth acting on the planar slip surfaces, as well as weight (W_i), and centrifugal (F_i) forces per unit depth on the sliding wedge are represented.

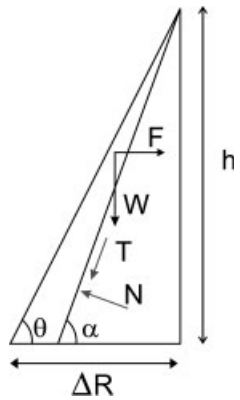

Figure 8. Theoretical simple wedge model for predicting the angle of the slope at high rotation velocities.

The fracture surface is assumed to be planar. Normal (N) and tangential (T), forces per unit depth acting on the slip surface, as well as weight (W) and centrifugal (F) forces per unit depth on the sliding wedge are represented.

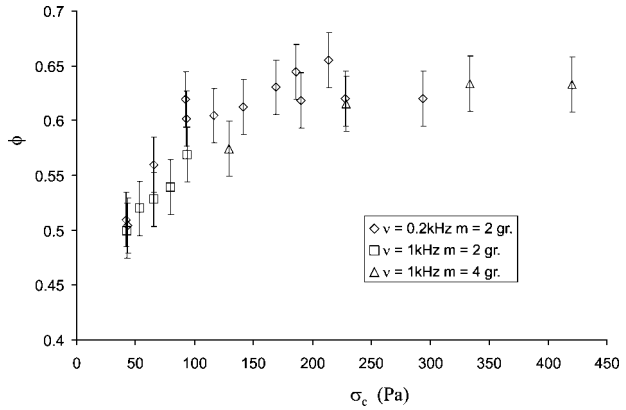

Figure 9. Experimental values of the particle volume fraction for previbrated samples as a function of the effective consolidation stress σ_c due to vibration.

The inset indicates the frequency v of previbration and the mass m of powder used. The error bars are calculated from the indeterminacy in measuring the bed height.

and normal forces per unit depth, respectively, on the slip plane. After integration, the ratio F/W is given by

$$\frac{F}{W} = \frac{\omega^2 R}{g}\left[1 - \frac{\Delta R}{3R}\tan\theta(\cot\theta + \cot\alpha)\right] \tag{2}$$

Equation 2 can be further simplified, since we observe experimentally that the sliding wedge is thin (see Figure 5), thus, we can make the approximation $\alpha \approx \theta$ and rewrite Eq. 2 as

$$\frac{F}{W} = \frac{\omega^2 R}{g}\left(1 - \frac{2\Delta R}{3R}\right) = \tan\chi \tag{3}$$

where we have defined and angle χ, which is a measure of the magnitude of the centrifugal force.

The slope is stable as long as $T < N \tan\varphi + Ch/\sin\alpha$, where h is the height of the slope. Applying the equilibrium condition, it follows

$$F(\cos\alpha - \tan\varphi\sin\alpha) - W(\sin\alpha + \tan\varphi\cos\alpha) < \frac{Ch}{\sin\alpha} \tag{4}$$

Using Eq. 3, Eq. 4 can be rewritten as

$$\sin(\alpha - \theta)\sin[\chi - (\alpha + \varphi)] < \frac{2C}{\rho g h}\cos\varphi\cos\chi\sin\theta \tag{5}$$

As the rotation velocity is increased, χ increases, and the lefthand side of Eq. 5 increases while the righthand side decreases. The critical yield condition is met when the left hand side of Eq. 5 reaches a maximum, which is obtained for

$$\sin\{[\chi - (\alpha + \varphi)] - (\alpha - \theta)\} = 0 \tag{6}$$

Using again the approximation $\alpha \approx \theta$, the value of the angle of internal friction φ can be derived from Eq. 6 as

$$\varphi = \chi - \alpha \tag{7}$$

Thus, φ is derived from the angle χ, which is calculated from experimental measurements of ω, ΔR, and α (Eq. 3). Note that the value of cohesion is not needed in Eq. 7 to derive the angle of internal friction. Thus, the procedure will consist of first deriving φ from experimental observations of the stable angle of the slope α and ΔR for a given ω in the range of high-rotation velocities. Once the angle of internal friction is obtained, the cohesion C will be found from the experimental value of the rotation velocity at which the first avalanche occurs, and using the model of wedges proposed in the theoretical analysis.

Experimental Results

From the sample volume we first obtain the average particle volume fraction (see Figure 9), showing an increase from around $\phi \simeq 0.5$ for the loosely packed nonvibrated bed to $\phi \simeq 0.64$ for the samples vibrated at the highest intensity, which conforms to the random close packing limit of hard spheres.[23]

Following the methodology previously described, we obtain the experimental values of the angle of internal friction φ from the measurement of the angle of the slope at high-rotation velocities. Results are shown in Figure 10. It can be seen that within the experimental scatter the values of φ do not depend on the rotation velocity employed for the calculation as should be expected. From these results it can be also inferred that the average angle of internal friction $\langle\varphi\rangle$ decreases slightly as previbration intensity is increased. This correlation is also seen in Figure 11 where we have plotted $\langle\varphi\rangle$ as a function of the effective consolidation $\sigma_c \simeq \sigma_{c0}(1 + \Gamma)$. It is observed that $\langle\varphi\rangle$ decreases from about 25^0 at low-consolidations to about 22^0 at the highest consolidations, although the experimental indeterminacy precludes us from a statistically significant conclusion. Nevertheless, note that the value of the angle of internal friction estimated for the nonvibrated sample (around 25^0) agrees with the average angle of internal friction derived from the yield loci measured using the ring shear tester (Figure 2b). Moreover, the result obtained form the ring shear tester also indicates a

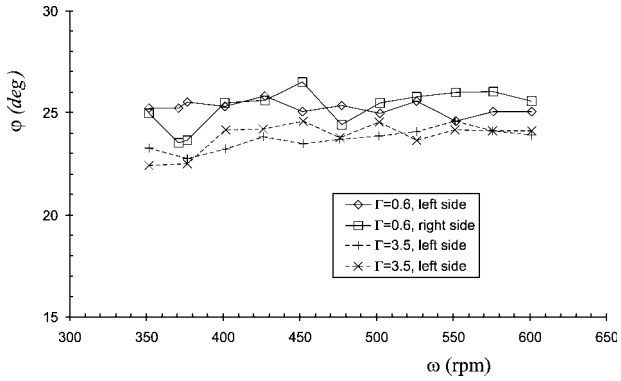

Figure 10. Values of the angle of internal friction φ for glass beads samples previbrated at different vibration intensities (indicated, v = 200 Hz).

Results (in the range of high-rotation velocities) are calculated from observations of the stable angle of the slope at both sides (left and right) of the rotating cell.

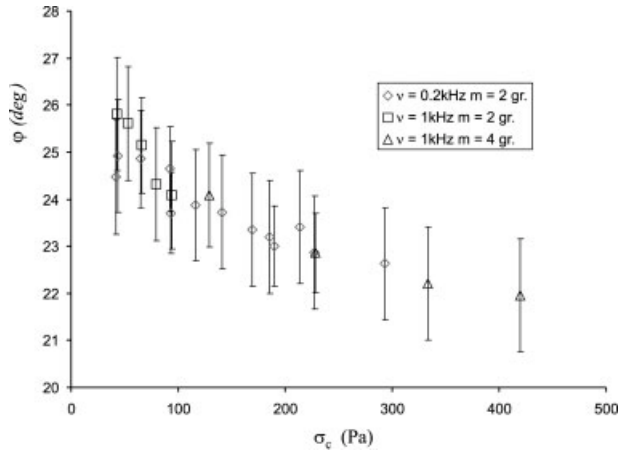

Figure 11. Experimental values of the angle of internal friction φ for previbrated samples as a function of the effective consolidation σ_c due to previous vibration.

The inset indicates the frequency v of previbration, and the mass m of powder used. [Color figure can be viewed in the online issue, which is available at www.interscience.wiley.com.]

decrease of $\langle\varphi\rangle$ as the maximum normal stress used to obtain the yield locus is increased. We cannot establish, however, a direct comparison between both sets of data since the effective consolidation stress defined in our experiment is not directly related to the maximum normal stress applied by the lid on the powder using the ring shear tester.

In Figure 12 we have plotted the experimental values of cohesion C obtained from the measurement of the rotation velocity at which the first avalanche is observed. It is seen that cohesion increases as the effective consolidation is increased due to previbration. This trend agrees with the tendency of observed using the ring shear tester (Figure 2b), albeit our apparatus is able to measure cohesion accurately in the range of smaller consolidations.

As a general conclusion, it can be said that compaction induced by previous vibration gives rise to a slight decrease of the average angle of internal friction accompanied by a significant increase of the cohesion of the powder. The effect of this change of material properties on powder flow at high rotation velocities in the CPT is shown in Figure 13. We compare photograms of samples rotated at the same velocity, but previbrated at different intensities. It is observed more powder remaining in the central core as cohesion is increased (see Figure 13). The slight decrease of the angle of internal friction hinders the stability of slopes in the rotating field, thus, we observe slightly steeper slopes for the samples previbrated at larger intensities (see Figure 13).

Concerning the shape of the theoretical slip surface for the first avalanche (Figure 7), it is difficult to infer information about the slip surface just from the post-avalanche surface profiles (Figure 3). It must be admitted that the slip surface indicated in Figure 7 is partly a matter of conjecture, since one section of the slip surface is exposed when the surface layer slides away, but the remaining section becomes buried by the avalanching powder. Moreover, as the rotation velocity keeps increasing, and the powder is heterogenous at the bulk level, it is likely that the very first avalanche involves only a weaker section of the wedge. The theoretical values derived for the depth of the avalanche are in the range between 0.5 cm and 0.8 cm, and increase as the previbration intensity is increased. Although we cannot establish a clear comparison with experimental results because of insufficient experimental determinacy, it is remarkable that the depth of the observed avalanches are also of the order of several millimeters. Let us note that in ref. 11 we analyzed the sliding of an inclined layer of cohesive powder by using the same wedge model as used in the this article, and we arrived at a similar conclusion. While the angle of inclination at which avalanche occurred was well defined, the depth of the avalanche was subject to higher indeterminacy, which was attributable to powder heterogeneity, and did not allow for a quantitative comparison with the theoretical prediction. Nevertheless, the cohesion values obtained in ref. 11 from the experimental angle of avalanche, and using the same wedge model employed in the this article, were in accordance with the cohesion directly measured by an independent technique.

Estimation of interparticle cohesion force

Using the Rumpf averaging Eq.,[24] the interparticle cohesion force f_t can be estimated as

$$f_t \sim \sigma_t \frac{\pi d_p^2}{\zeta \phi} \tag{8}$$

where σ_t (tensile strength) is the maximum tensile stress that the powder can withstand, and ζ is the coordination number (average number of contacts per particle). The coordination number ζ can be related to the particle volume fraction ϕ by the Eq. $\zeta \simeq (\pi/2)\,(1-\phi)^{-3/2}$ (ref. 25). Experimental tests on fine powders using a ring shear tester[15] and a tilted fluidized-bed technique[26] have shown that the yield locus of cohesive

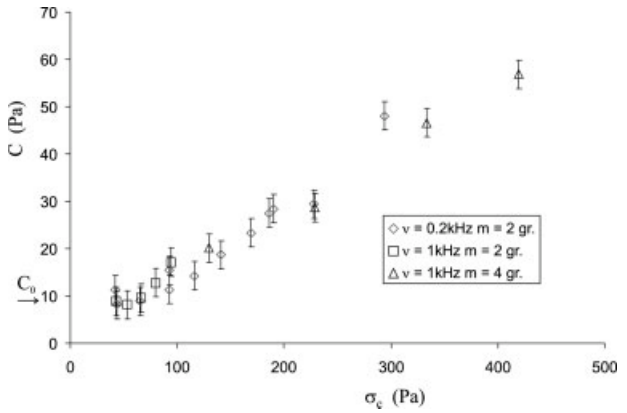

Figure 12. Average experimental values of cohesion C for previbrated samples as a function of the effective consolidation stress σ_c, which is increased by previous vibration.

The inset indicates the frequency v of previbration and the mass m of powder used. The arrow in the vertical axis indicates the cohesion $C_0 \simeq 10$ Pa measured for the non-vibrated samples, subjected to a consolidation stress just due to their own weight $\sigma_{c0} \simeq 40$ Pa. [Color figure can be viewed in the online issue, which is available at www.interscience.wiley.com.]

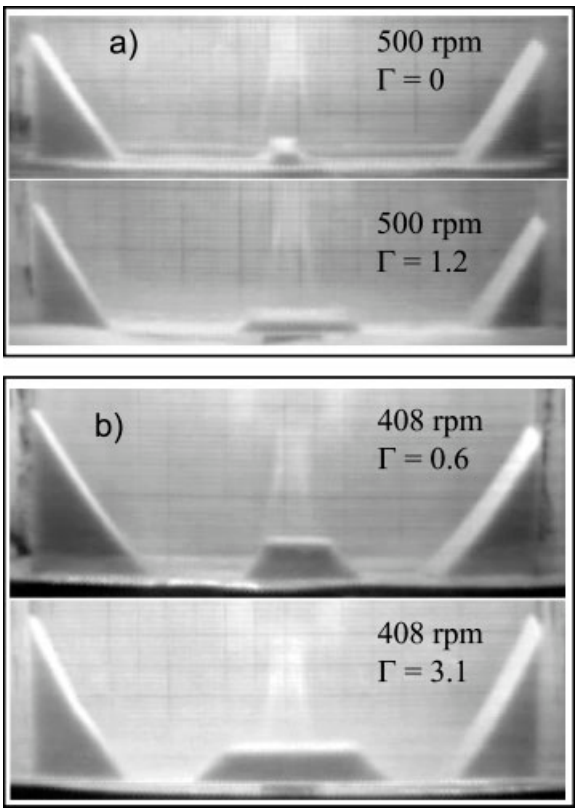

Figure 13. (a) Photograms taken at a rotation velocity ω = 500 rpm for a non vibrated 2 grams sample (top), and for a previbrated sample (bottom, Γ = 1.2, ν = 1 kHz); (b) the same phenomenon is observed for this 4 grams sample rotated at ω = 408 rpm.

The top photogram corresponds to a previbration intensity of Γ = 0.6, while for the bottom photograph Γ = 3.1. Note that for the previbrated sample the angle of the slope is slightly larger (indicating smaller angle of internal friction), and there is more material resting in the core zone (indicating higher cohesion).

powders has a convex shape at very small and negative values of σ. As a first approximation, we will consider that the tensile strength σ_t, and the cohesion C are of the same order of magnitude ($C \sim \sigma_t$).

Likewise, the average consolidation force f_c transmitted to the interparticle contacts by the effective consolidation stress σ_c can be estimated as

$$f_c \sim \sigma_c \frac{\pi d_p^2}{\zeta \phi} \tag{9}$$

Estimations of the cohesive force between particles f_t as a function of the interparticle consolidation force f_c are plotted in Figure 14. The data shows that, in the range of forces tested, f_t increases with f_c in about one order of magnitude, indicating that the increase of cohesion C at the bulk level is mainly attributable to the increase of the cohesive force at the microlevel of interparticle contacts.

Discussion

Calculation of interparticle cohesion force

For dry particles the interparticle attractive force arises mainly from van der Waals and capillary interaction. The van der Waals attractive force is produced by the interaction of fluctuating molecular dipole fields. Assuming that retardation effects are negligible and that the interaction between molecules is pairwise, Hamaker[27] summed up all the interactions between two spherical and rigid particles at contact with dia. d_1 and d_2, and arrived at the approximate expression for the attractive force

$$f_{vdW} \simeq \frac{Ad^*}{12z_0^2} \tag{10}$$

where A is the Hamaker constant ($A \simeq 1.5 \times 10^{-19}$ J for glass[28]), $d^* = d_1 d_2/(d_1 + d_2)$ is the reduced particle diameter, and $z_0 \simeq 3$–4 Å is the distance of closest approach between two molecules. Because of the short range of the molecular interaction, the van der Waals force is actually determined by the local radius of curvature of the surface asperities at contact. Therefore the typical size of the surface asperities d_a must be used in Eq. 10 instead of the particle diameters. A typical value reported for the size of surface asperities of fine powder particles is $d_a \simeq 0.2$ μm,[29–31] which agrees with the average asperity diameter derived from AFM analysis of the surface of glass beads.[32] Thus, we can estimate $f_{vdW} \sim 10$ nN for our experimental particles.

The experiments are carried out at ambient conditions and it, is, therefore, possible that moisture condensation at the asperities at contact yield attractive capillary forces. The capillary force between two equal spheres of radius r can be approximated by $f_{cl} \simeq \pi \gamma r^2 \beta/S$, where γ is the liquid surface tension, β is the half-filling angle, and S is the separation distance.[33] For small water bridges $S \simeq r\beta$, we can write f_{cl}

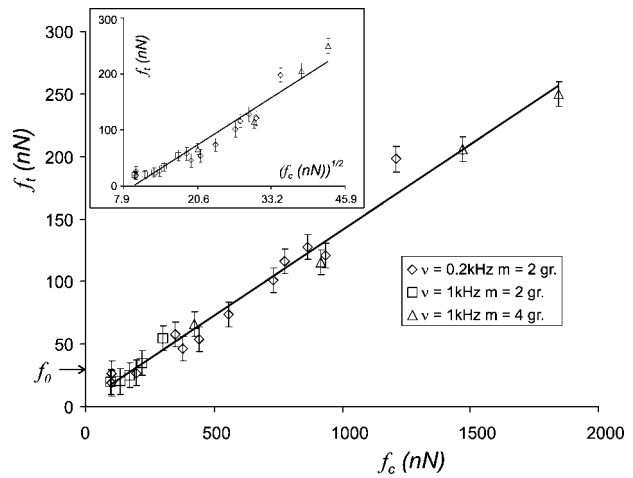

Figure 14. Estimated interparticle cohesion force as a function of the estimated interparticle consolidation force caused by previous vibration.

The arrow in the ordinate axis indicates the interparticle force calculated by summation of the van der Waals and capillary forces. The inset is a plot of the interparticle cohesion force as a function of the square root of the interparticle consolidation force. The straight line is a linear fit to the data ($R^2 = 0.938$).

$\simeq \pi\gamma r$, where $r \sim d_a/2 \simeq 0.1$ μm and $\Gamma = 72.75$ mN/m. Accordingly, the contribution to adhesion by the capillary force is $f_{cl} \simeq 20$ nN. The total attractive force expected would be $f_0 = f_{vdW} + f_{cl} \simeq 30$ nN, in agreement with the cohesive interparticle force estimated from our measurements for the loosely packed samples (see Figure 14). It must be remarked, however, that it is quite difficult to estimate accurate values of the interparticle force since it can fluctuate strongly due to its dependence on the surface roughness of the particles, and the likely presence of force chains.

In the case of elastic contact deformation, the interparticle cohesion force should not depend on previous consolidation. This is in contrast to our results and to most of the experimental results with fine cohesive powders.[34] The reason is that even small consolidation stresses may induce plastic deformation of the surface asperities at contact, thus, enhancing the interparticle cohesive force.[35] The critical load on the contact P_Y for the initiation of plastic yield within the bulk of the particle can be calculated as[36]

$$P_Y \simeq \frac{2\pi^3 (d_a^*)^2 Y^3}{3E^2} \tag{11}$$

where Y is the compressive yield strength, E is the Young modulus, and d_a^* is the reduced asperity diameter. For contacts between asperities of same size $d_a^* = d_a/2$. In the case of contact of the particle with a flat surface $d_a^* = d_a$.

Using as typical values $Y = 1100$ MPa (reported for glass[37]), and $E = 68.9$ GPa (reported for soda-lime glass[37]), it is estimated $P_Y \simeq 20$ nN, which is lower than the smallest consolidation forces that we estimate in our experiments (see Figure 14). At higher pressures the plastic zone extends from the bulk of the particle until it reaches the contact surface and propagates along it. Mesarovic and Johnson[38] have proposed the relationship

$$f_t \simeq \frac{3\sqrt{\pi}}{2} \frac{wE^*}{H^{3/2}} \sqrt{f_c} \tag{12}$$

where $1/E^* = 2(1 - \nu^2)/E$, being ν the Poisson ratio ($\nu = 0.16$ for soda-lime glass[37]), $w = 2\gamma$ is the work of adhesion, being γ the surface energy of the solid ($\gamma \simeq 0.3$ J/m^2 for glass[32,39]), and $H \approx 3Y$ is the hardness of the solid material. This equation clearly shows the important role of local deformations of the contact area on adhesion, and, thus, the relevance of material hardness on the cohesive behavior of the fine powder. It must be noted that Eq. 12 is just approximate since it is only valid in the so called "fully plastic regime", in which the region of plastic deformation is as large as the contact area, with the maximum radius of the contact area much smaller than the local radius of curvature. In order to arrive to Eq. 12, Mesarovic and Johnson considered that the material deforms elastically when the force is decreased during the pull-off process (fully plastic deformation with elastic recovery), and that the area at detachment is much smaller than the area at pull-on.[38] Though there exist improved models that relate f_t to f_c,[40] and given the uncertainty in the calculation of the contact forces from the bulk stresses estimated in this work, Eq. 12 is enough accurate for our purpose of checking the reliability of the experimental results obtained from our measuring device. The interested reader will find a detailed review on contact mechanics theory in ref. 41. The best linear fit to data of f_t vs. $\sqrt{f_c}$ (see inset of Figure 14) yields a slope of 6.65 (nN)$^{1/2}$, which agrees in order of magnitude with the values predicted by Eq. 12 (the calculated slope is 9.41 (nN)$^{1/2}$) using $w = 0.6$ J/m^2, $E = 68.9$ GPa, $\nu = 0.16$ and $H = 3300$ MPa.

Estimation of the granular Bond number

A further advantage of estimating the interparticle cohesive force is that we can calculate the granular Bond number Bo_g of the bed compacted by vibration, defined as the ratio of interparticle cohesion force f_t to particle weight w_p. Generally, it can be said that Bo_g is a good predictor of flowability. Nase et al.[42] found that the static angle of repose of a granular heap did not depend on particle size if the particle weight exceeded the interparticle cohesion force ($Bo_g \lesssim 1$), but increased markedly as Bo_g was increased above one. Just as with the static heap angle, a sharp decrease was observed to occur in the discharge rate through a hopper when Bo_g was increased above one.[42] Figure 15 is a plot of Bo_g as a function of the effective consolidation σ_c of the previbrated bed. As seen in this graph, the flowability of samples compacted by vibration can be seriously hampered. For example, the granular Bond number may increase by one order of magnitude for a 2 grams sample vertically vibrated at five times the gravity acceleration. Figure 15 also shows that the data of Bo_g vs. σ_c is well fitted by the power law $Bo_g \simeq 22.8\,(\sigma_c/\sigma_{c0})^{1.15}$, where $\sigma_{c0} \simeq 40$ Pa is the minimum consolidation stress just due to sample self-weight. It must be noted, however, that this result is restricted to vertical vibrations of small intensity that cause powder compaction. In other situations, such as application of large vibration intensities[2] or horizontal excita-

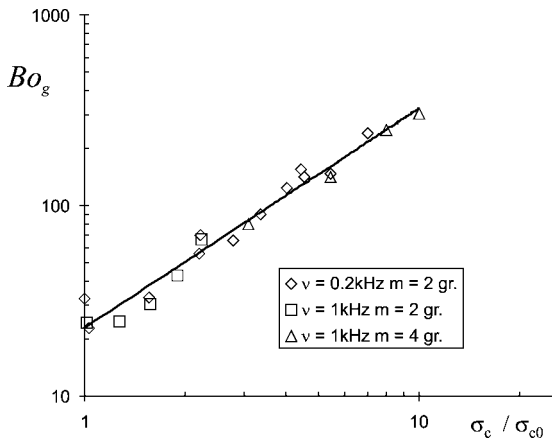

Figure 15. Granular Bond number, defined as the ratio of interparticle cohesion force to particle weight, for samples of fine glass beads as a function of the effective consolidation σ_c, due to previous vibration (made nondimensional with the smallest consolidation stress corresponding to sample weight per unit area $\sigma_{c0} \simeq 40$ Pa).

The solid line is the best fit of the data to a power law ($Bo_g \simeq 22.8\,(\sigma_c/\sigma_{c0})^{1.15}$).

tion,[12] vibration may have indeed the opposite consequence, thus helping to improve the flow behavior of powders.

Conclusions

In this article, we have used a centrifuge powder tester to obtain the angle of internal friction φ, and cohesion C of fine glass beads as affected by previous vibration in the vertical direction. In the experimental procedure we use a small amount of mass, typically between 2 and 4 grams, contained in a rectangular cell. The bed is initialized and subjected to low-intensity vertical vibrations of controlled frequency v and amplitude A for a fixed period of two minutes. By means of previbration the material becomes compacted. Then the cell is taken to the centrifugal powder tester, in which it is rotated around its vertical axis at increasing values of the rotation velocity. At a critical point the shear stress caused by the action of the centrifugal force is large enough to drive material avalanches. From a theoretical analysis of these avalanches, based on the Coulomb's method of wedges we derive the angle of internal friction and cohesion of the glass beads. These parameters have been also measured using an independent standard technique (automated Schulze ring shear tester) that served us to check that the material behavior conforms to the Coulomb yield condition. Moreover, the cohesion and angle of internal friction obtained using the ring shear tester agree within the experimental indeterminacy, with the values obtained from our centrifuge powder tester. Some advantages of the centrifuge powder tester are: (1) it needs a quite reduced mass of material for testing, (2) the test is of short duration, typically of the order of minutes, (3) the shear on the sample is not induced by external mechanical parts, which avoids problems, such as wall sliding, (4) the fracture inside the sample is clearly identified by direct visualization of the shearing process, and, (5) it allows for testing at very small consolidations.

Measurements using the centrifuge powder tester have been performed using different masses previbrated at different frequencies and amplitudes. Results from the tests are fitted to a single trend when they are plotted as a function of the effective consolidation stress imposed on the bed by means of previbration $\sigma_c = \sigma_{c0}(1+\Gamma)$, where σ_{c0} is the self-weight consolidation, and $\Gamma = A(2\pi v)^2/g_0$ is the ratio of vibrational to gravitational acceleration. Basically, the data indicate a significant increase of cohesion and a slight decrease of the angle of internal friction as the effective consolidation on the sample is increased. The interparticle cohesion force f_t has been estimated from the cohesion measured, and using the averaging Rumpf's equation. For the unconsolidated samples, the value estimated for f_t agrees with the expected force due to the sum of van der Waals and capillary forces for undeformed contacts between surface asperities. However, the interparticle cohesion force increases as previbration intensity is increased, being this the main reason for the increase of cohesion at the bulk level. According to theoretical estimations, the increase of the interparticle cohesion force is attributable to the plastic yield of the surface asperities at contact. The rate of increase of the interparticle cohesion force with the interparticle consolidation force is in accordance with the results predicted by a theoretical model on plastic contacts between surface asperities. It can be concluded that fine powder flowability is seriously hindered by compaction due to previbration. In the range of previbration intensities applied the granular Bond number, defined as the ratio of interparticle cohesion force to particle weight, is increased by one order of magnitude.

Acknowledgments

We are indebted to Dr. M. A. S. Quintanilla, who helped us in performing measurements using the Schulze tester. This research has been supported by Xerox Foundation, Spanish Government Agency Ministerio de Ciencia y Tecnologia (contract FIS2006-03645) and Junta de Andalucia (contract FQM 421).

Literature Cited

1. Nowak ER, Knight JB, Povinelli ML, Jaeger HM, Nagel SR. Reversibility and irreversibility in the packing of vibrated granular material. *Powder Technol*. 1997;94(1):79–83.
2. Thomas B, Mason MO, Squires AM. Some behaviors of shallow vibrated beds across a wide range in particle size and their implications for powder classification. *Powder Technol*. 2000;111(1–2):34–49.
3. Faraday M. On a peculiar class of acoustical figures; and on certain forms assumed by groups of particles upon vibrating elastic surfaces. *Phil Trans R Soc London* 1831;121:299–340.
4. Knight JB, Fandrich CG, Lau CN, Jaeger HM, Nagel SR. Density relaxation in a vibrated granular material. *Phys Rev E*. 1995;51: 3957–3963.
5. Ennis BJ. *Unto Dust Shalt Thou Return, Powders & Grains*. Behringer and Jenkins, eds., Balkema, Rotterdam; p. 13, 1997.
6. Quintanilla MAS, Valverde JM, Castellanos A, Viturro RE. Looking for self-organized critical behavior in avalanches of slightly cohesive powders. *Phys Rev Lett*. 2001;87:194301(1–4).
7. Schwedes J. Fließverhalten von Schüttgütern in Bunkern. Verlag Chemie GmbH, Weinheim (1968). ASTM D6128-06 Standard test method for shear testing of bulk solids using the Jenike Shear Cell, ASTM International.
8. Nedderman RM. *Statics and Kinematics of Granular Materials*. Cambridge University Press; UK; 1992.
9. Coulomb CA. Mémoires de Mathématics et de Physique présentés à l'Académie des Sciences par divers savants et lus dans les assemblées, année 1773. p. 343 (Paris 1776).
10. Ancey C. Plasticity and geophysical flows: A review. *J Non-Newton Fluid Mech*. 2007;142:4–35.
11. Valverde JM, Castellanos A, Ramos A, Watson PK. Avalanches in fine, cohesive powders. *Phys Rev E*. 2000;62:6851–6860.
12. Kollmann TH, Tomas J. Effect of applied vibration on silo hopper design. *Part Sci Technol*. 2002;20:15–31.
13. Roberts AW, Scott OJ. An investigation into the effects of sinusoidal and random vibrations on the strength and flow properties of bulk solids. *Powder Technol*. 1978;21:45–53.
14. Arnold PC, Kaaden KS. Reducing hopper wall friction by mechanical vibration. *Powder Technol*. 1977;16:63–66.
15. Schulze D, Wittmaier A. Flow properties of highly dispersed powders at very small consolidation stresses. *Chem Eng Technol*. 2003;26:133–137.
16. ASTM D6773-02, Standard shear test method for bulk solids using the Schulze Ring Shear Tester, ASTM International.
17. Svarovsky L. *Powder Testing Guide: Methods of Measuring the Physical Properties of Bulk Powders*. Elsevier Applied Science, England; 1987.
18. Schwedes J. Review on testers for measuring flow properties of bulk solids. *Granular Matter*. 2003;1–43.
19. Castellanos A, Quintanilla MAS, Valverde JM. Method and device for measuring the angle of friction and the cohesion of granular media. Patent no. WO 2007/042585 A3. University of Seville Spain; April 19; 2007.
20. Castellanos A, Quintanilla MAS, Valverde JM, Soria-Hoyo C. Novel instrument to characterize dry granular materials at low consolidations. *Rev Sci Instrum*. 2007;78:073901(1–10).
21. Evesque P, Rajchenbach J. Instability in a sand heap. *Phys Rev Lett*. 1989;62(1):44–46.
22. Atkinson JH. *Introduction to the Mechanics of Soils and Foundations*. McGraw Hill International, UK (1993).

23. Makse HA, Johnson DL, Schwartz LM. Packing of compressible granular materials. *Phys Rev Lett*. 2000;84:4160–4163.
24. Rumpf H. Grundlagen and methoden des granulierens. *Chemie Ing Techn*. 1958;30:144–158.
25. Suzuki M, Makino K, Yamada M, Iinoya K. Study on the coordination number in a system of randomly packed, uniform-sized spherical particles. *Int Chem Eng*. 1981;21:482–488.
26. Castellanos A, Valverde JM, Quintanilla MAS. The Sevilla Powder Tester: A tool for characterizing the physical properties of fine cohesive powders at very small consolidations. *KONA Powder and Particle* 2004;22:66–81.
27. Hamaker HC. The London-Van der Waals attraction between spherical particles. *Physica* 1937;4:1058–1072.
28. Visser J. On Hamaker constants: a comparison between Hamaker constants and Lifshltz - van der Waals constants. *Adv Coll Inter Sci*. 1972;3:331–363.
29. Krupp H. Particle adhesion- theory and experiment. *Adv Coll Inter Sci*. 1967;1:111–239.
30. Massimilla L, Donsi G. Cohesive forces between particles of fluidized-bed catalysts. *Powder Technol*. 1976;15:253–260.
31. Rietema K. *The Dynamics of Fine Powders*. Elsevier, London; UK 1991.
32. Schaeffer DM, Carpenter M, Gady B, Reifenberger R, DeMejo LP, Rimai DS. Surface roughness and its influence on particle adhesion using atomic force techniques. In: Rimai DS, DeMejo LP, Mittal KL, eds. *Fundamentals of adhesion and interfaces*. VSP, Utrecht, The Netherlands; 1995:35–48.
33. Willett CD, Adams MJ, Johnson SA, Seville JPK. Capillary bridges between two spherical bodies. *Langmuir*. 2000;16:9396–9405.
34. Molerus O. The role of science in particle technology. *Powder Technol*. 2002;122:156–167.
35. Rimai DS, DeMejo LP, Mittal KL, eds. *Fundamental of adhesion and interfaces*. VSP, Utrecht, The Netherlands; 1995.
36. Vu-Quoc L, Zhang X, Lesburg L. Normal and tangential forcedisplacement relations for frictional elasto-plastic contact of spheres. *Int J Solids Struct*. 2001;38:6455–6489.
37. http://www.matweb.com. Source: ASM Engineered Materials Reference Book, Second Edition, Michael Bauccio, Ed. ASM International, Materials Park, OH; 1994.
38. Mesarovic SD, Johnson KL. Adhesive contact of elastic-plastic spheres. *J Mech Phys Solids* 2000;48:2009–2033.
39. Kinloch AJ. In: *Adhesion and Adhesives: Science and Technology*. Chapman and Hall, New York; 1987:26–34.
40. Gilabert FA, Quintanilla MAS, Castellanos A, Valverde JM. Adhesive elastic plastic contact: theory and numerical simulation. *Z Angew Math Mech*. 2007;87(2):128–138.
41. Castellanos A. The relationship between attractive interparticle forces and bulk behaviour in dry and uncharged fine powders. *Adv Phys*. 2005;54:263–376.
42. Nase ST, Vargas WL, Abatan AA, McCarthy JJ. Discrete characterization tools for cohesive granular material. *Powder Technol*. 2001; 116:214–223.

Appendix A: Critical Equilibrium Equations for the Wedge Model

The forces per unit depth acting on the two subwedges that compose the wedge are shown in Figure 6. W_1 and W_2 ($W_1 = W_2 = W$) are the weight forces per unit depth of each sub-wedge. F_1 is the centrifugal force per unit depth acting on subwedge 1, and F_2 is the centrifugal force per unit depth acting on subwedge 2. Integration over the area of each subwedge gives

$$F_1 = \frac{1}{24}\rho\omega^2 \tan\beta(2R + d)(R - d)^2 \tag{A1}$$

$$F_2 = \frac{1}{24}\rho\omega^2 \tan\beta(R + 2d)(R - d)^2 \tag{A2}$$

$$W = \frac{1}{8}\rho g \tan\beta(R - d)^2 \tag{A3}$$

where R is the radius of the rotating cell and ρ is the bulk density. On each subwedge the condition of static equilibrium must apply (i.e., the sum of forces must equal zero). Also, along each slip surface the Coulomb yield condition must be satisfied. Thus, we have a total of nine equations

$$F_1 - N_1 \sin\beta - T_1 \cos\beta + N_3 = 0 \tag{A4}$$

$$F_2 + N_2 \sin\beta - T_2 \cos\beta - N_4 = 0 \tag{A5}$$

$$N_1 \cos\beta - T_1 \sin\beta - W_1 - T_3 = 0 \tag{A6}$$

$$N_2 \cos\beta + T_2 \sin\beta - W_2 + T_4 = 0 \tag{A7}$$

$$T_1 = N_1 \tan\varphi + \frac{1}{2}C(R - d)\sec\beta \tag{A8}$$

$$T_2 = N_2 \tan\varphi + \frac{1}{2}C(R - d)\sec\beta \tag{A9}$$

$$T_3 = N_3 \tan\varphi + \frac{1}{2}C(R - d)\tan\beta \tag{A10}$$

$$N_3 = N_4 \tag{A11}$$

$$T_3 = T_4 \tag{A12}$$

where T_i and N_i represent tangential and normal forces per unit depth, respectively, on the slip planes, and W_i and F_i are the weight and centrifugal forces per unit depth, respectively, as indicated in Figure 6. Equations A4 to A12 must be satisfied with eight unknowns T_1, T_2, N_1, N_2, T_3, N_3, T_4, and N_4. Solving for the condition of compatibility, it is obtained

$$\Omega(\beta, d) = \frac{f_1 + 24\kappa f_2/(1 - \varsigma)}{(2 + \varsigma)f_3 + (1 + 2\varsigma)f_4} \tag{A13}$$

where

$$\Omega = \frac{\omega^2 R}{g_0}$$

$$\kappa = \frac{C}{\rho g_0 R}$$

$$\varsigma = \frac{d}{R}$$

$$f_1 = 6\sin\varphi\,(\cos 2\varphi + \sin^2\beta)$$

$$f_2 = \frac{\cos\varphi\cos\beta}{\sin\beta}\,(\cos 2\varphi + \sin^2\beta)$$

$$f_3 = \cos(\beta + \varphi)\cos(\beta - 2\varphi)$$

$$f_4 = \cos(\beta - \varphi)\cos(\beta + 2\varphi)$$

The minimum of $\Omega(\beta,d)$ gives the rotation velocity at which the first avalanche is theoretically predicted for given values of the cohesion and angle of internal friction.

Manuscript received July 27, 2007, and revision received Dec. 3, 2007.